Chapter IV

$BaZrO_3$/Poly (Vinylidene difluoride) Ceramic Nanocomposite Films with Improved Dielectric and Energy Storage Properties

4.1 Introduction

As discussed in chapter I, with the global energy consumption demand for power generation in the last few decades, it is a matter of importance to develop renewable energy sources to fulfil the demand. The dielectric capacitors with high charge discharge capabilities, long life and low cost are required in high power energy storage applications[169–172]. In recent years, polymer-based composites have attracted researcher's mind because of its high dielectric breakdown strength, flexibility, extraordinary dielectric properties and high energy storage density[173–176]. High value of maximum polarization, low remanent polarization and high dielectric breakdown strength are necessary key parameter for a dielectric material to have high energy storage density. Polymers have high breakdown strength (E_b) and less dielectric constant. Among the various polymers, PVDF polymer due to its ferroelectric nature have highest dielectric constant (~10) and has been used in present composite as a matrix[2]. There are two types of polymers have been reported polar and nonpolar on the basis of mean dipole moment. Polar polymers have higher dielectric constant whereas nonpolar polymers have lower dielectric constant. PVDF polymer have four different crystalline phases namely α, β, γ and δ out of which α phase is nonpolar because of T G T G (T-Trans, G-Gauche) conformation and β phase is polar form of α phase having TTTT conformation[177–180]. On the other hand, ceramics have lower dielectric strength, difficult processing and brittleness inspite of having better dielectric permittivity. Hence, to overcome the limitations of polymers and ceramics, researchers have focused in last few decades to improve the dielectric properties of polymers with the introduction of ceramic fillers into polymer matrix in order to develop flexible ceramic - polymer composites with high dielectric strength[116,181,182]. However, introduction of ceramic nanoparticles to the polymer matrix leads to enhancement of local electric field resulting in decrease in dielectric breakdown strength of the nanocomposites[91]. Also,

according to percolation theory, if the fraction of nanoparticles is increased beyond limit, it leads to formation of conducting path along the polymer matrix resulting in failure of the dielectric materials. Therefore, the fraction of filler nanoparticles must be limited. The nanoparticles having high surface energy and absence of strong interaction with polymeric chain leads to agglomeration and separation of phase from the polymer matrix results in non-uniformity throughout the film. In order to overcome the problem, surface modification of ceramic nanoparticles has been carried out to ensure better interaction with polymeric chain to get homogeneous dispersion. The improved interaction between the polymer matrix and the ceramic filler is mainly responsible for the improved dielectric behaviour which is the necessary parameter to improve the energy storage property of the composites.

In past decades, researchers have focused much effort in the development of lead free materials for such application due to the hazardous effect of Lead on environment. Among various lead free dielectrics, ferroelectrics have been used for energy storage application due to its large dielectric constant. $BaZrO_3$ having ferroelectric behaviour, high thermal stability, high melting temperature and tunable dielectric properties have attracted the attention of researchers [183,184]. In the current research work, we have tried to synthesize surface hydroxylated $BaZrO_3$/PVDF nanocomposite for energy storage application. Surface modification has been carried out using hydrogen peroxide (H_2O_2) and its effect on electrical properties has been studied. The energy storage property has been studied using PE hysteresis curve.

4.2 Synthesis of BZ/PVDF composite film

Barium Zirconate (BZ) ceramic powders were prepared using high energy ball mill technique. Alfa Aesar reagents of $BaCO_3$ and ZrO_2 were taken in stoichiometric amount and ball milling was performed in acetone media for 24 hr with the help of zirconia balls

as grinding media. After ball milling, mixture was dried at 80^0C for 12 hr and calcined at 1250^0C for 6 hr after crushing the powder using agate mortar to form the single-phase solid solution of $BaZrO_3$.

BZ/PVDF nanocomposite was synthesized by solution casting method. For this purpose, 90 wt. % of PVDF and 10 wt. % of BZ nanoparticle were separately dispersed in Di-methyl formamide (DMF) solvent using ultra Sonicator[141]. Then the above solutions were mixed together in a beaker and magnetically stirred for 8-12 hours continuously so that BZ nano powders get dispersed uniformly throughout the polymer solution. The solution was casted in a Petri dish and dried at 120 ℃ in an oven for 12 hrs in order to obtain a homogeneous film. Pure PVDF film was also synthesized by above mentioned solution casting method in order to compare the properties. Surface hydroxylation of BZ nano powder was done using hydrogen peroxide solution to ensure better dispersion and homogeneity of ceramic fillers into the polymer matrix. For this purpose, 10 wt. % of BZ was taken in a beaker and 20 ml H_2O_2 was added in it. Then the above solution was refluxed at 106℃ for 6 hrs and then dried at 120℃ for 10 hrs. FTIR spectroscopy analysis was performed to confirm the surface hydroxylation of BZ nano powder. Now, above surface modified powder was dispersed in DMF solvent and the above-mentioned solution casting method was followed in order to prepare film. Thus pure PVDF film, BZ/PVDF and hy-BZ/PVDF composite films were prepared using solution casting method. The flow chart for the synthesis of BZ particles is shown in Fig. 4.1 and process of solution casting method for composite synthesis is shown in Fig. 4.2.

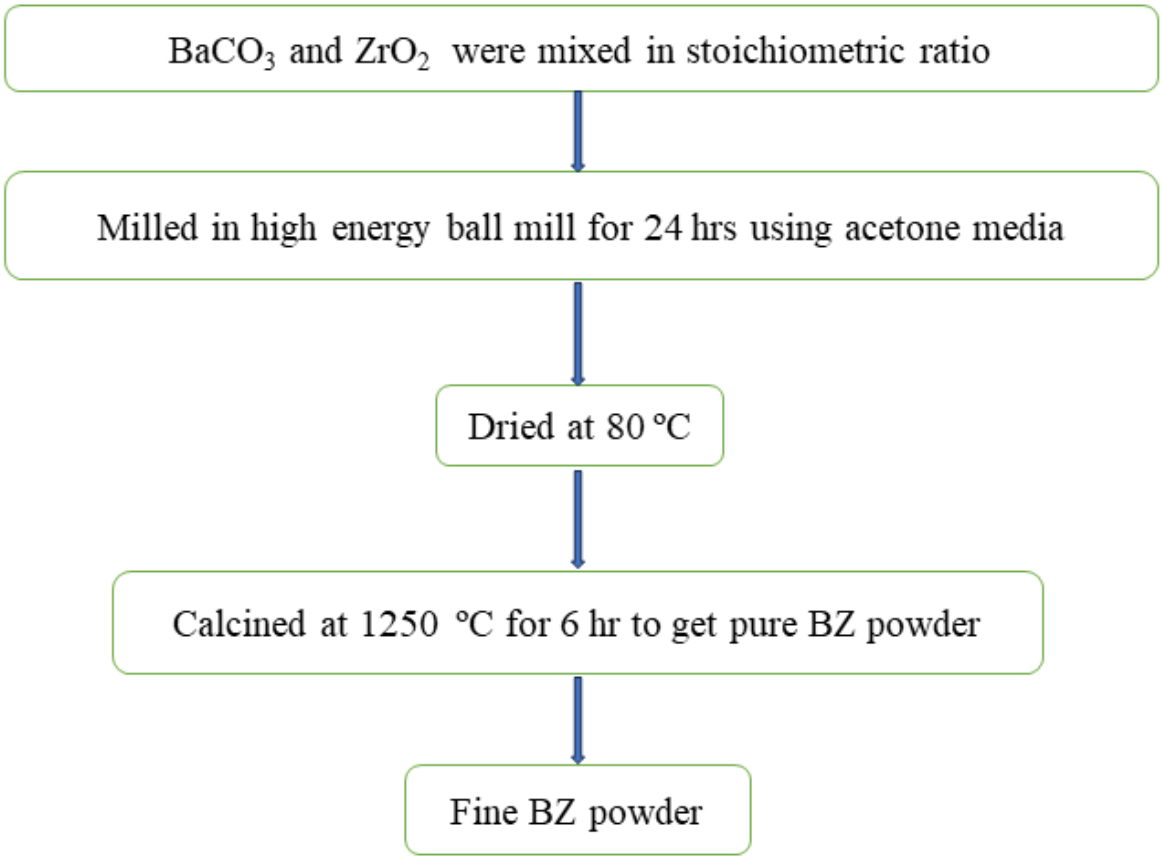

Fig. 4.1 Flowchart for Synthesis of BZ particles using High Energy Ball Mill process

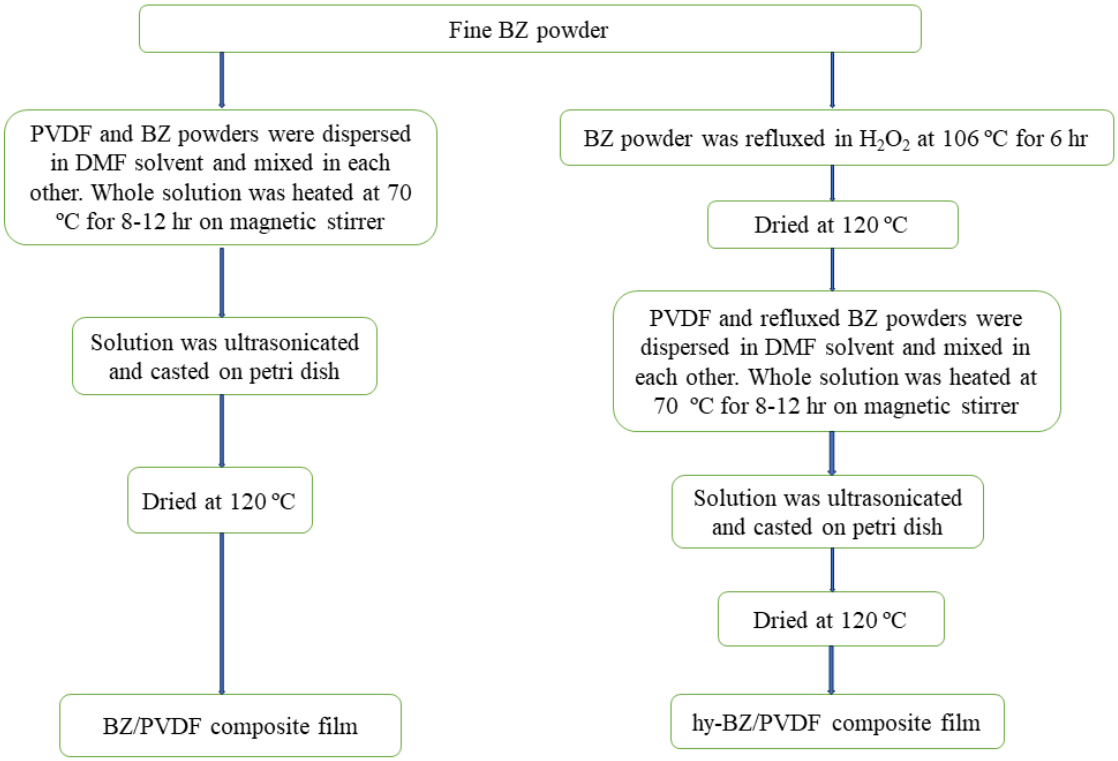

Fig. 4.2 Synthesis process of BZ/PVDF and hy-BZ/PVDF composite using solution casting method

4.3 Results and discussion

XRD pattern of BZ/PVDF nanocomposites were analyzed in the angle (2θ) range of 10-60^0 using Rigaku Smartlab benchtop X-Ray Diffractometer in order to verify the successful formation of composite. TGA -DSC analysis was carried out to know the idea about thermal stability nature of composites. Electroding was performed on both sides of each composites using air dried silver paste for the measurements of dielectric properties and the measurements were performed in the temperature range 30℃ to 120℃ at different frequency range. For PE hysteresis curve measurement, electroding was also performed with air dried silver paste and measurement was performed at room temperature at 40 Hz frequency via varying electric field. Electric breakdown strength measurement was

performed with the help of AC dielectric breakdown experimental setup followed by Weibull analysis.

4.3.1 X-ray Diffraction Analysis

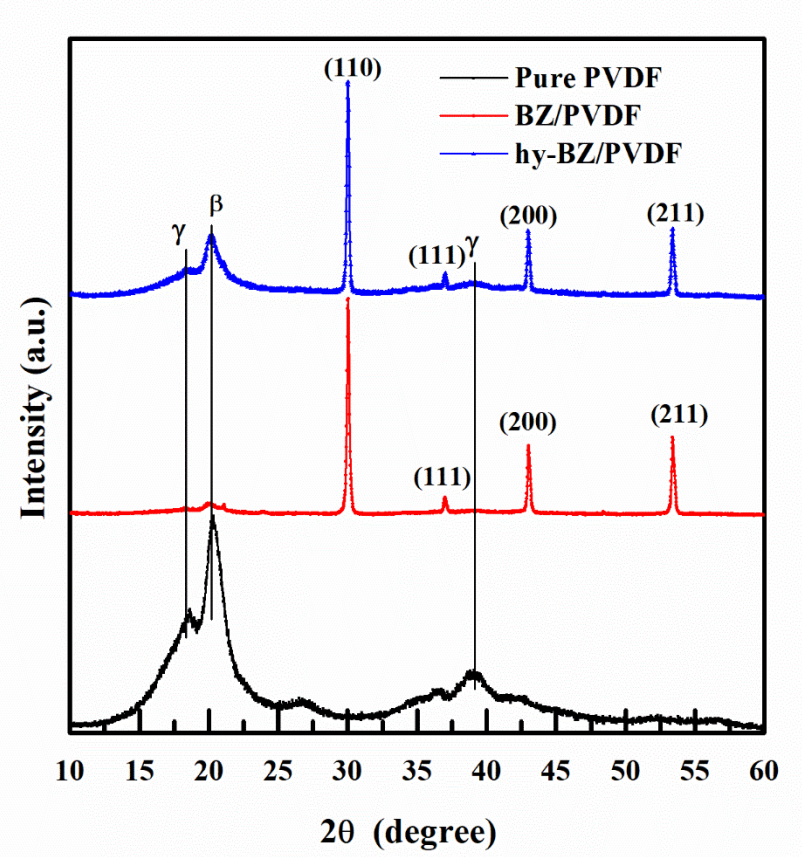

Fig. 4.3 XRD pattern of Pure PVDF film, BZ/PVDF and hy-BZ/PVDF composite film

X-ray diffraction analysis was performed to know the crystalline nature of PVDF film, BZ/PVDF film and hydroxylated BZ/PVDF film and can be seen in Fig. 4.3. The XRD pattern of pure PVDF film shows high intensity peaks at angles (2θ) 18.6^0, 26.6^0, 52.5^0 predominantly α-phase, 20.3^0, 36.5^0 and 39.2^0 represents β and γ-phase of PVDF respectively same as reported in previous reported literature[10,107,141]. PVDF film represents semicrystalline nature. XRD pattern of BZ/PVDF and hy-BZ/PVDF that shows intense peak at 2θ 21^0 (100), 30^0 (110), 37^0 (111), 43^0 (200) and 53^0 (211) are corresponding to

perovskite structure of BZ nanoparticles[184] as well as peak at 2θ corresponding to 18.3^0 and 20.3^0 are assigned as γ and β phases of PVDF .Thus nanocomposite film has peaks corresponding to the peaks of BZ powder as well as peaks corresponding to the dominant polar phase of PVDF which confirms successful formation of composite film. XRD was recorded for analysis of crystalline structure of three different films: PVDF film, BZ/PVDF film, and hydroxylated BZ/PVDF film. These peaks are consistent with previously reported literature and indicate that the PVDF film has a semicrystalline nature and have crystal structure. The presence of the peaks corresponding to the BZ powder indicates as cubic perovskite structure with Pm3m space group. Thus, the BZ crystals are present in the composite film and are integrated with the PVDF film, forming a single and cohesive material**.**

4.3.2 FTIR Analysis

FTIR analysis has been carried out to verify the successful hydroxylation of BZ powder. For this purpose, FTIR spectra was recorded for hydroxylated BZ powder as shown in the Fig. 4.4. Hydroxylated BZ powder shows peak at 1386 cm^{-1} and 3435 cm^{-1} which is corresponding to -OH peaks as reported in available literature[141]. Thus, FTIR spectra of hydroxylated BZ confirms the successful hydroxylation of BZ powder. FTIR spectra of hydroxylated BZ powder shows peaks at 534 cm^{-1} and 1545 cm^{-1} which are corresponding vibrational stretching of Zr-O bonds and vibrational modes of Ba-O bonds respectively[185]. FTIR spectra of pure PVDF film, BZ/PVDF film and hy-BZ/PVDF film have absorption peaks corresponding to α, β and γ phases of PVDF that is clearly visible. Absorption peaks corresponding to wave number 836 cm^{-1}, 876 cm^{-1}, 1236 $cm^{-1}$are assigned as γ, 1071 cm^{-1},1166 cm^{-1} are assigned as β and absorption peaks corresponding to 1400 cm^{-1} are assigned as α phase of PVDF polymer. These results are according to previously reported literature on PVDF based nanocomposites[186].

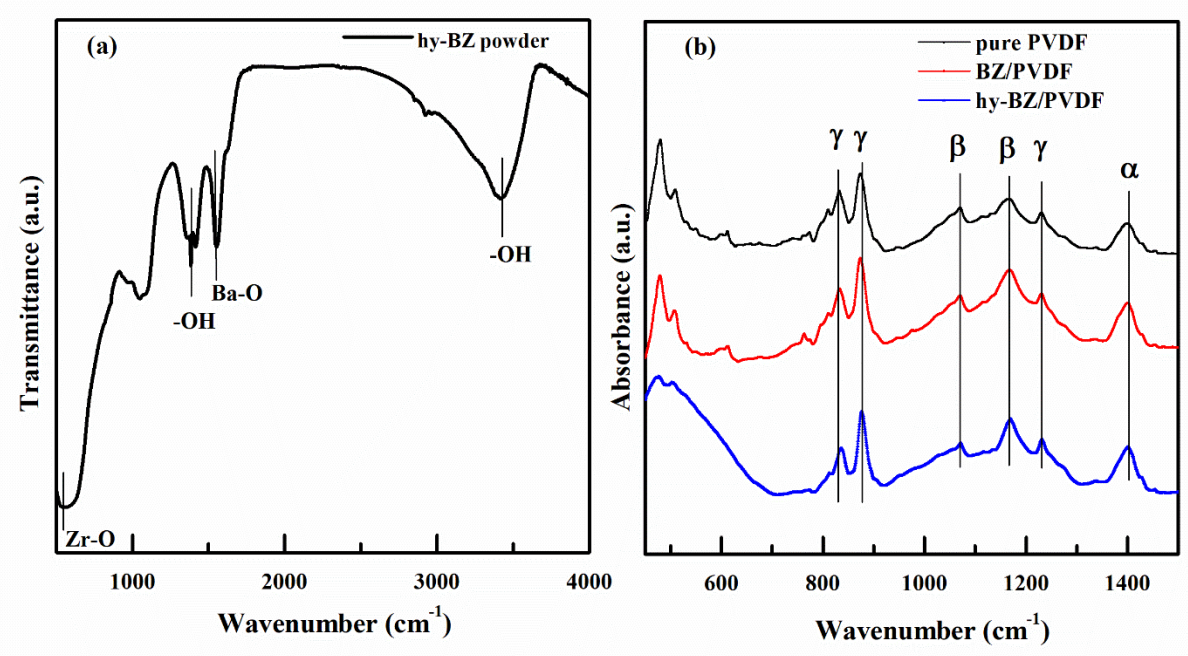

Fig. 4.4 FTIR spectra of (a) hydroxylated BZ powder, (b) pure PVDF, BZ/PVDF and hy-BZ/PVDF composite

4.3.3 Thermal analysis using TGA and DSC

Thermogravimetric analysis (TGA) was done to check the thermal stability of composite film. There was no weight loss in the TGA plot up to 450 ^{0}C and there after a sharp declination occurs which shows the mass loss of the composites. This means that after 450 ^{0}C an endothermic process takes place which might be due to dissociation of ceramic filler from the polymer matrix and pyrolysis of PVDF polymer. This result is identical with previously reported data[141,187]. From the TGA plot of BZ/PVDF and hy-BZ/PVDF, it can be seen in Fig. 4.5 that weight loss of upto 90 % occurs for both the composites which is exactly equal to the wt. % of PVDF polymer in composites. It might be due to the complete pyrolysis of PVDF polymer and removal of PVDF polymer from the composite.

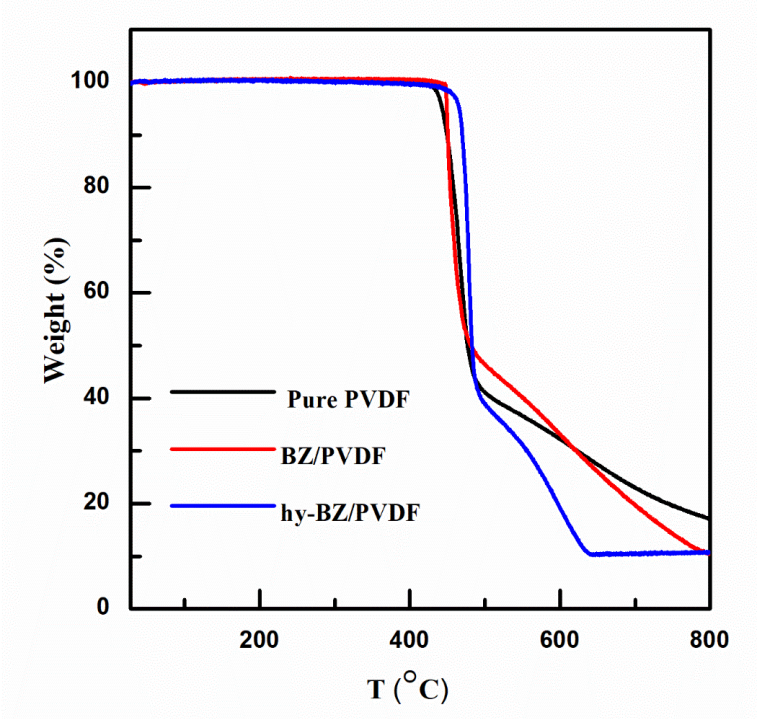

Fig. 4.5 TGA curve of pure PVDF, BZ/PVDF and hy-BZ/PVDF composite

Differential scanning calorimetry (DSC) analysis was performed to determine the nature of reaction takes place upon heat treatment. DSC plot shows the endothermic peak at 167 ^{0}C, 167.5 ^{0}C, 168.3 ^{0}C for pure PVDF, BZ/PVDF and hy-BZ/PVDF composite film respectively which is shown in Fig. 4.6. This successive increment in the value of melting temperature represents that hy-BZ/PVDF composite have increased electroactive phases of PVDF polymer[188,189]. The area under the curve of endothermic peak is higher in case of composites in comparison to PVDF polymer which represents higher degree of crystallinity of composites in comparison to pure PVDF film[190].

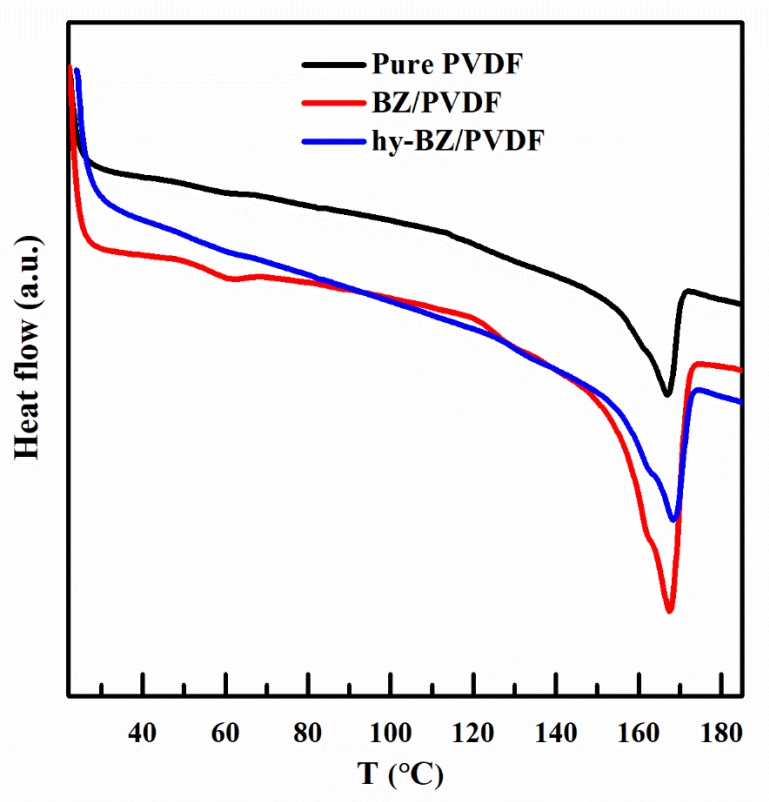

Fig. 4.6 DSC curve of pure PVDF, BZ/PVDF and hy-BZ/PVDF composite

4.3.4 Microstructural Analysis

Surface morphology of pure PVDF film and composite films has been analyzed using FESEM micrograph as shown in Fig. 4.7. Fig. 4.7(a) represents FESEM micrograph of hy-BZ nanopowder and its average particle size is found to be 59 nm using Image J software. In Fig. 4.7(b) spherulites are observed in case of pure PVDF film. In Fig. 4.7(c) lumps of ceramic can be observed on film surface and spherulites are clearly not visible in case of BZ/PVDF nanocomposite film which suggest that nonuniform distribution of ceramics in PVDF polymer matrix due to agglomeration of ceramic particles. To minimize the agglomeration and uniform distribution of ceramics in polymer matrix, surface hydroxylation of BZ ceramics using H_2O_2 has been performed before using it in PVDF polymer matrix for synthesis of polymer ceramic nanocomposite. In Fig. 4.7(d) lumps of ceramics are not visible and spherulites are clearly visible in case of hy-BZ/PVDF

nanocomposite film which suggest that surface hydroxylated BZ nanoparticles are uniformly distributed in PVDF polymer matrix. The FESEM result indicate that there is stronger interaction between PVDF polymer and hy-BZ nanoparticles in comparison to PVDF polymer and BZ nanoparticles. Thus better compatibility between hy-BZ nanoparticles and PVDF polymer is originated due to surface hydroxylation of BZ nanoparticles using H_2O_2. The presence of Ba, Zr and O can be observed in hy-BZ/PVDF nanocomposite film using elemental mapping analysis which is shown in Fig. 4.7(e-i).

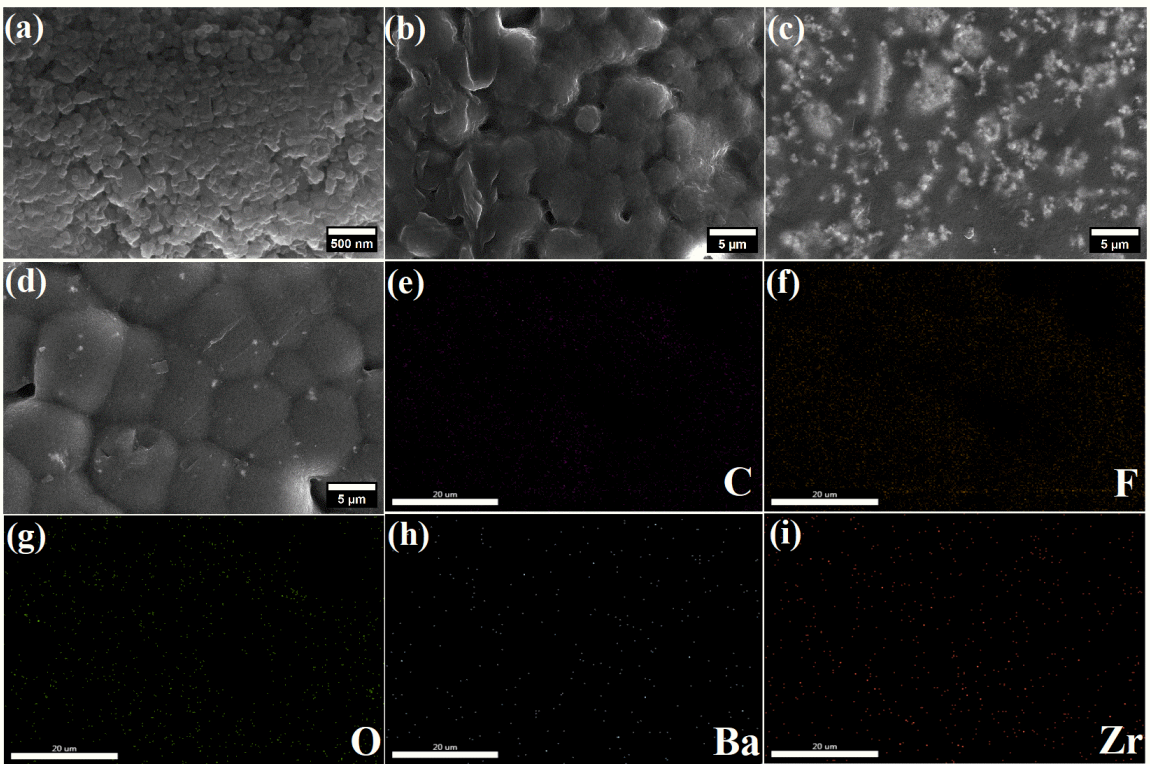

Fig. 4.7 FESEM image of (a) hy-BZ powder, (b) PVDF film, (c) BZ/PVDF film, (d) hy-BZ/PVDF composite film, (e-i) Elemental mapping of hy-BZ/PVDF composite film

4.3.5 X-ray photoelectron spectroscopy Analysis

The Fig. 4.8(a-h) depicted for elemental analysis for BZ/PVDF and hy-BZ/PVDF composite film. In the Fig. 4.8(a-b) O1s spectra the single peak is depicted at binding energy 531.45 eV and 531.46 eV for BZ/PVDF and hy-BZ/PVDF composite film respectively, and these photoelectron peaks are attributed to surface lattice oxygen and surface adsorbed oxygen with exhibiting O^{2-} oxidation state in the prepared system as previously also reported [141,191]**.** In the Fig. 4.8(c-d) chemical state of Ba3d shown at two different binding energy for both the samples as such at 794.77 eV, 779.40 eV binding energy for hy-BZ/PVDF film and 794.76 eV, 779.47 eV binding energy for BZ/PVDF film, where greater binding energy is attributed to $Ba3d_{3/2}$ and lower binding energy is attributed to $Ba3d_{5/2}$ spin orbit state. It is also determined that the Barium is exhibiting with a stable Ba^{2+} oxidation state as previously reported [192,193]**.** The Fig. 4.8(e-f) depicted for the XPS spectra of F1s with two separated peak F1 and F2 two different binding energy for both the samples as such shown, for hy-BZ/PVDF composite film the binding energies are 687.24 eV, 683.23 eV and binding energies 687.23 eV, 683.70 eV are for the BZ/PVDF film. Where the F1 is attributed to higher binding energy and F2 is attributed to lower binding energy and it can be say that peak at higher bonding energy (F1) is attributed to ion bonding Fluorine groups like F-C and F3-C species and lower bonding energy (F2) is attributed to either semi-covalent-bonding fluorine groups or formation of metal fluoride which may be $ZrF3$[194,195]**.** The Fig. 4.8(g-h) are shown for the photo electron spectra of Zr3d which is depicted as $Zr3d_{3/2}$ and $Zr3d_{5/2}$ for the higher and lower bonding energies respectively. Two spectra peaks are observed for the hy-BZ/PVDF at binding energy 183.9 eV and 177.76 eV and for BZ/PVDF composite film at binding energy 177.35 eV with a shift of peaks at higher binding energy and observed at 182.20 eV and 185.96 eV. With the previous

reported data, it can be concluding that Zr^{0} for metallic, Zr^{3+} for sub-oxides and Zr^{4+} for stoichiometric oxide [196,197].

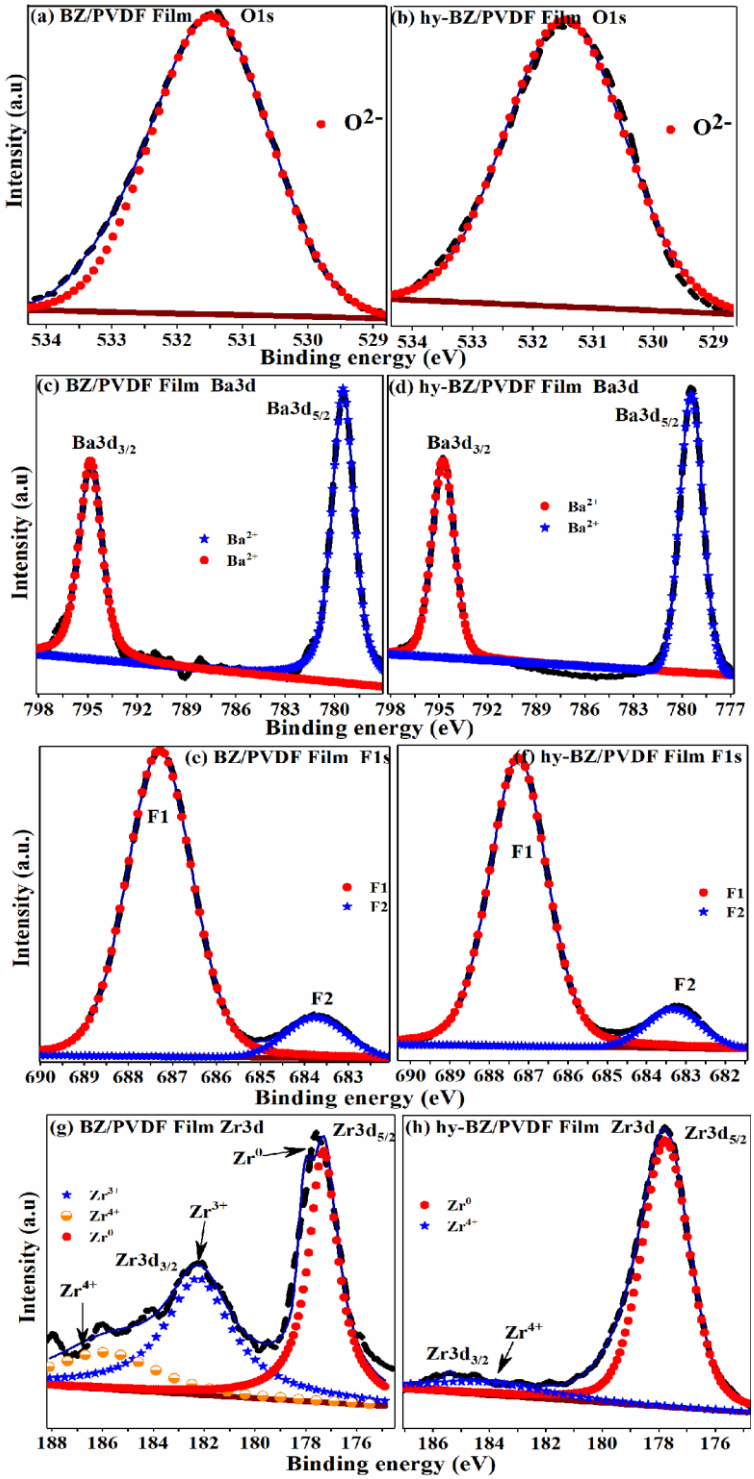

Fig. 4.8 (a-h) X-ray Photoelectron spectra of BZ/PVDF and hy-BZ/PVDF film.

4.3.6 Atomic Force Microscopy Analysis

Fig. 4.9 illustrates the Atomic Force Microscopy (AFM) image featuring 3D plot of the PVDF, BZ/PVDF and hy-BZ/PVDF nanocomposite film. In Fig. 4.9, surface roughness of the film is evident. For detailed analysis, we utilized Nova Px 3.0.4 rev software to depict the roughness characteristics as seen in Fig. 4.10. Pure PVDF represents more roughness than PVDF-based nanocomposites**.** The roughness of the BZ/PVDF shows higher value in comparison to pure PVDF film and hy-BZ/PVDF nanocomposite film which may be due to nonuniform distribution of BZ nanoparticles in the PVDF matrix. The roughness of the hy-BZ/PVDF nanocomposite film is lower in comparison to BZ/PVDF film due to uniform distribution of BZ particles in PVDF matrix and higher in comparison to pure PVDF film due to increased average grain size as can be seen in FESEM image. The root mean square roughness (R_{rms}) measurements indicate that PVDF has an Rrms of 6.5 nm while BZ/PVDF and hy-BZ/PVDF nanocomposite film has an Rrms of 9.1 nm and 8.7 nm respectively as shown by the yellow line in the inset of Fig. 4.10 (a-c).

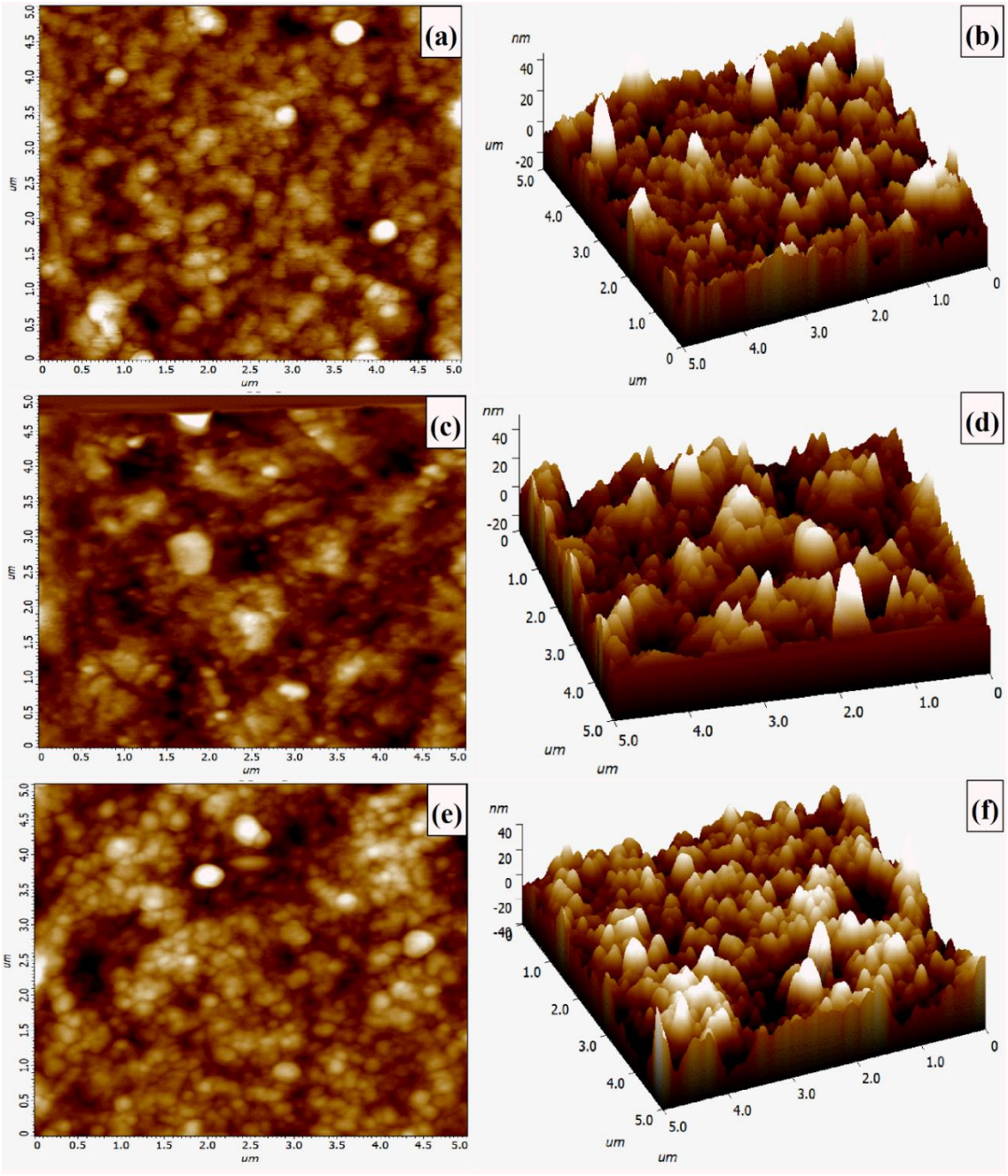

Fig. 4.9 (a) AFM micrograph (5x5 μm) of Pure PVDF film, (b) 3D AFM micrographs (5x5 μm) of Pure PVDF, (c) AFM micrograph (5x5 μm) of BZ/PVDF film, (d) 3D AFM micrographs (5x5 μm) of BZ/PVDF film, (e) AFM micrograph (5x5 μm) of hy-BZ/PVDF film, (f) 3D AFM micrographs (5x5 μm) of hy-BZ/PVDF film

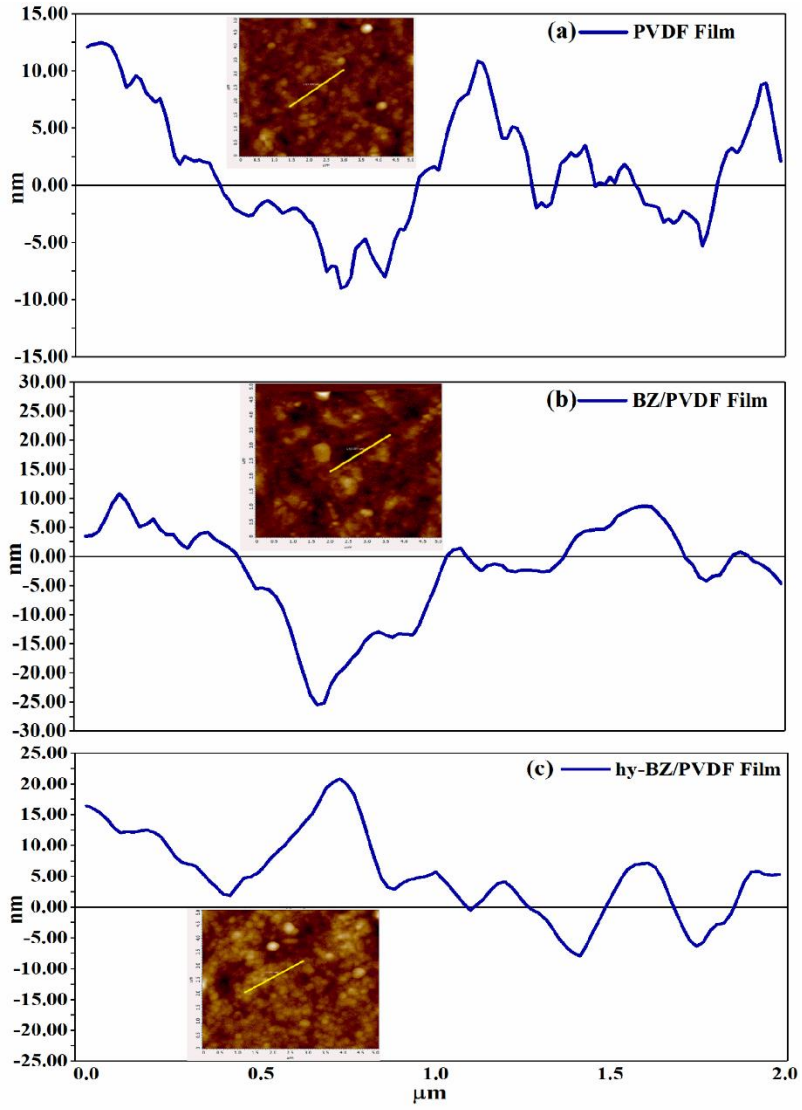

Fig. 4.10 Roughness profile of (a) Pure PVDF film, (b) BZ/PVDF, (c) hy-BZ/PVDF film

4.3.7 Dielectric properties

The temperature variation of dielectric constant and tanδ is shown in Fig. 4.11 for PVDF, BZ/PVDF and hy-BZ/PVDF nanocomposites at 1KHz frequency in temperature range 30-120℃. The dielectric permittivity of pure PVDF film, BZ/PVDF and hy-BZ/PVDF film shows simultaneous increasing behavior with temperature. Large increment in the value of permittivity is achieved beyond 80℃ due to enhanced mobility of the molecules at elevated temperature[198]. The value of dielectric loss of pure PVDF film as well as composites are almost same at room temperature but at higher temperature BZ/PVDF composite have less

dielectric loss and hy-BZ/PVDF composite have higher dielectric loss in comparison to pure PVDF film. The dielectric constant has been much improved in case of hy-BZ/PVDF (ε_r ~26) in comparison to pure PVDF film (ε_r ~8) on the introduction of hydroxylated ceramic nanofiller in PVDF polymer matrx at room temperature. This remarkable enhancement in the value of dielectric constant might be due to the higher dielectric constant of BZ ceramic. Thus nanocomposites have significantly enhanced dielectric constant with dielectric loss approximately same as in case of PVDF film at room temperature. The temperature dependance of dielectric constant at different frequencies has been studied for BZ/PVDF and hy-BZ/PVDF composites which is shown in Fig. 4.11. The dielectric constant and dielectric loss decreases with increasing frequency for composites and is almost stable for 100 KHz – 1MHz frequency range. The dielectric loss is associated with polarization mechanism, dipole relaxation for both component of composites and resonance of the polymer matrix[121,168,199]. Ceramic nanofillers shows generally lower dielectric loss in comparsion to polymer at a given frequency[200–202].

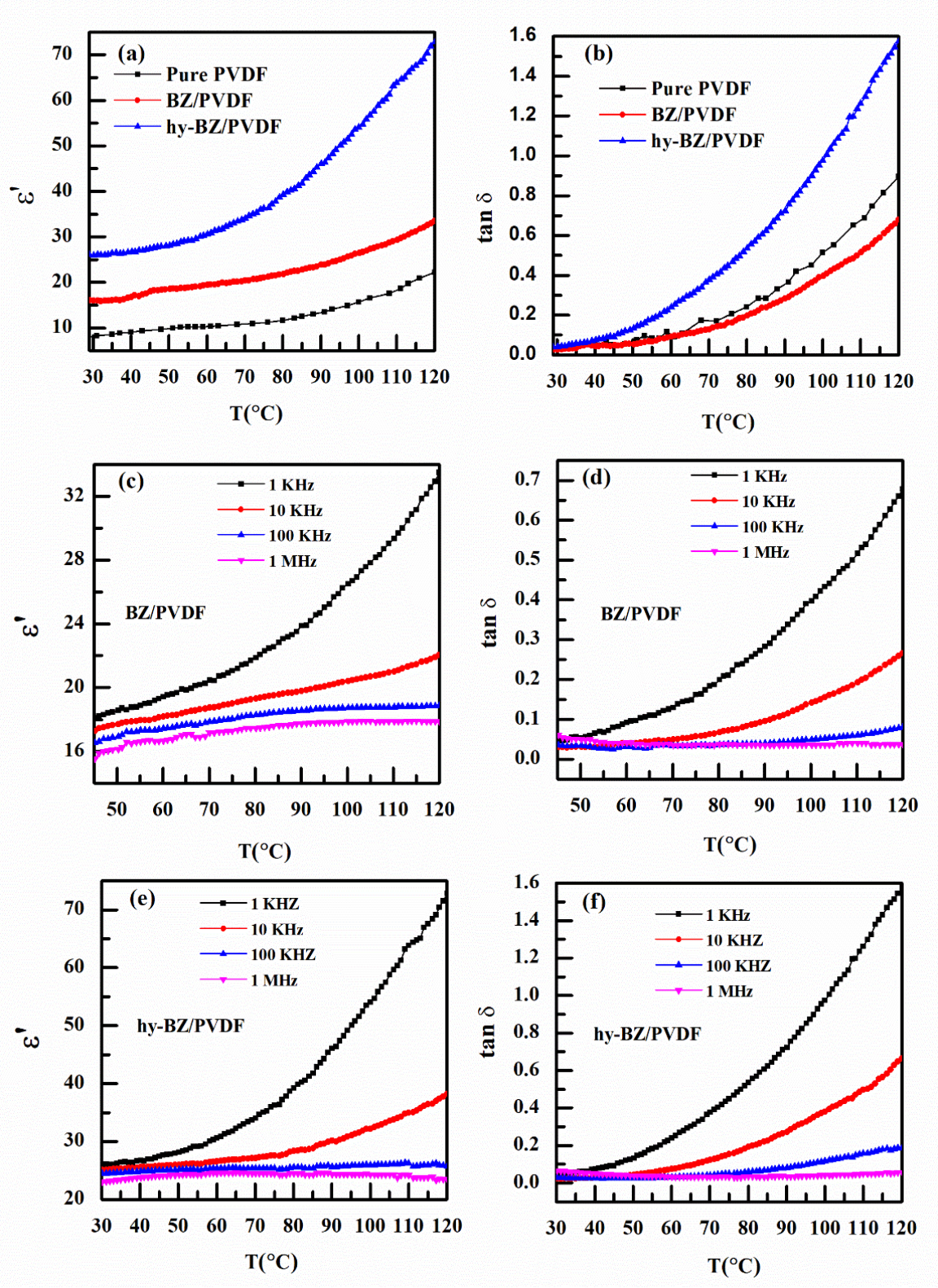

Fig. 4.11 temperature dependance of dielectric constant and dielectric loss (a),(b) for pure PVDF, BZ/PVDF and hy-BZ/PVDF composites, and at different frequencies for (c),(d) BZ/PVDF composite and (e), (f) hy-BZ/PVDF composite

4.3.8 P-E hysteresis loop Analysis:

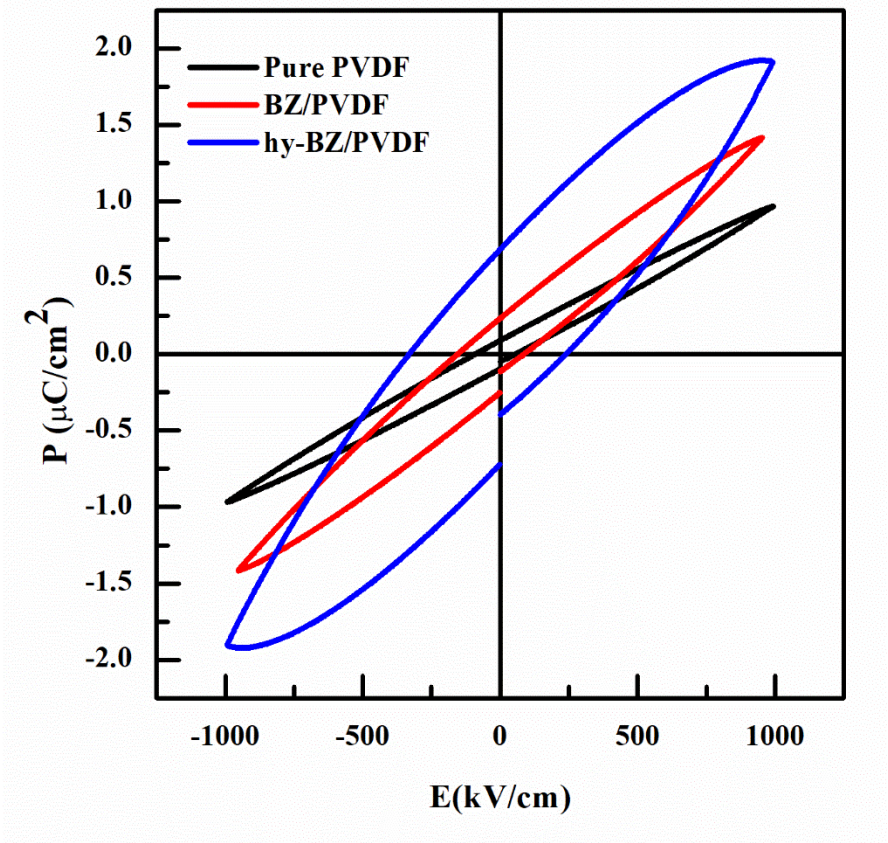

Fig. 4.12 PE hysteresis loop for pure PVDF film, BZ/PVDF and hy-BZ/PVDF composite

Fig. 4.12 shows PE hysteresis curve for PVDF film, BZ/PVDF composite film and hy-BZ/PVDF composite film at 40 Hz frequency. The pure PVDF film shows low value of polarization due to non-polar α-phase. Introduction of the BZ nanoparticles into the polymer matrix increases the value of polarization due to the ferroelectric nature of BZ nano powder. The remanent polarization was also increased but the area $\int EdP$ was increased significantly which shows improvement in energy density of the nanocomposite in comparison to pure PVDF film making it more suitable for energy storage application. Now in case of hy-BZ/PVDF nanocomposite, increment in polarization value is observed for the same value of electric field of BZ/PVDF composite. This enormous increase in the polarization value might be attributed to the more electroactive phase of PVDF, which being polar in nature. The value of polarization is found to be increasing with increasing

electric field. No sign of saturation is there till application of 950 kV/cm field indicates that the nanocomposite can exert electric field much higher than this applied electric field. The value of the remnant polarization and maximum polarization at 950 kV/cm for pure PVDF film, BZ/PVDF and hy-BZ/PVDF composite film is shown in table 4.1. The energy storage density can be determined qualitatively from PE hysteresis curve by area under the curve and Paxix that is listed in table 4.1 for pure PVDF, BZ/PVDF and hy-BZ/PVDF film.

Table 4.1 Remnant Polarization (P_r) , Maximum Polarization (P_m), Energy storage density (U_e) and discharge efficiency (η) of pure PVDF film, BZ/PVDF and hy-BZ/PVDF composite film

S. No.	Sample Name	Remnant Polarization P_r ($\mu C/cm^2$)	Maximum Polarization P_m ($\mu C/cm^2$)	Energy Storage density U_e (J/cm^3)	Discharge efficiency η (%)
1.	Pure PVDF	0.08	0.92	0.47	82
2.	BZ/PVDF	0.23	1.41	0.77	66
3.	hy-BZ/PVDF	0.68	1.92	1.11	43

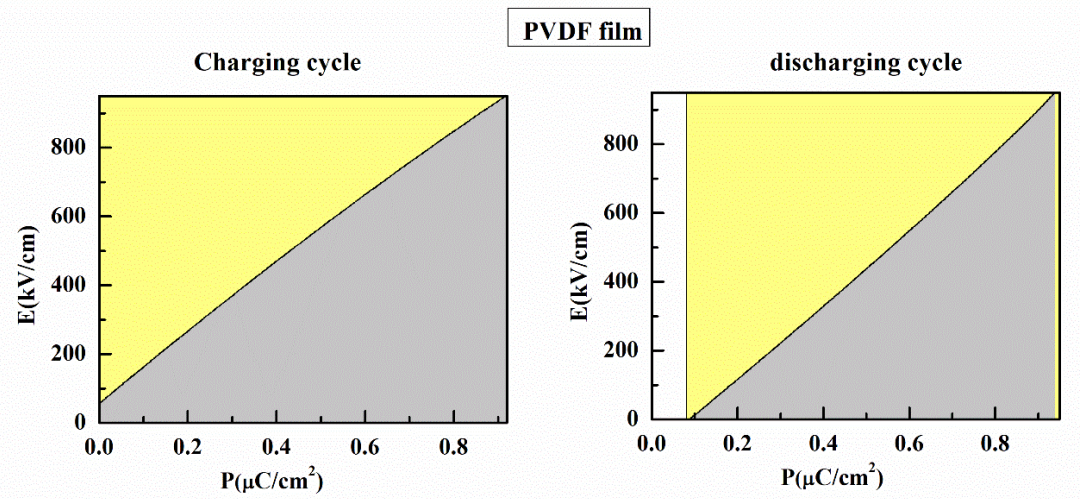

Fig. 4.13 Partial PE hysteresis loop response for calculation of energy density for PVDF film

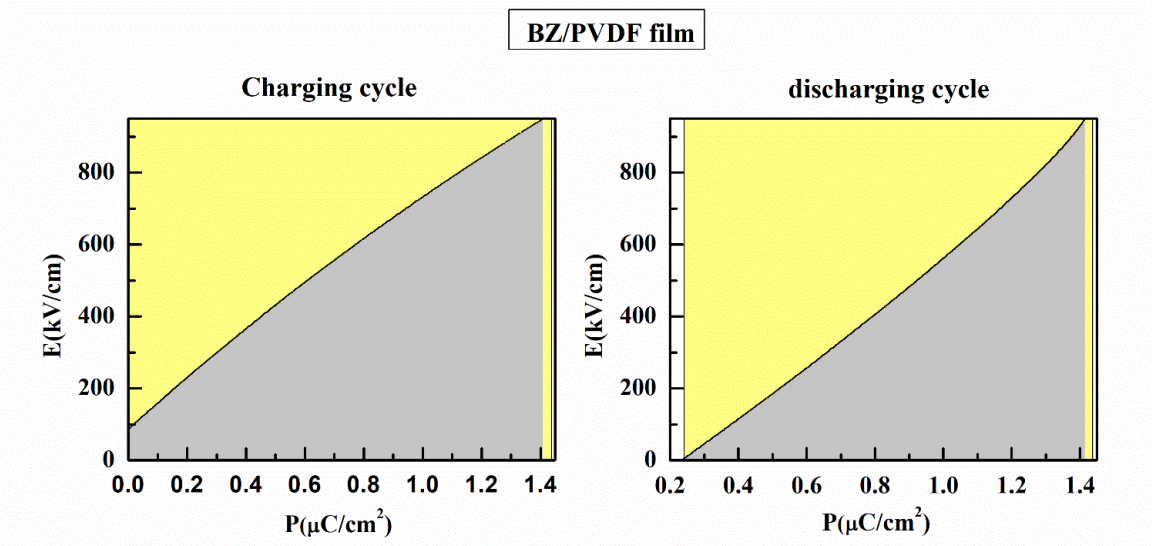

Fig.4.14 Partial PE hysteresis loop response for calculation of energy density for BZ/PVDF film

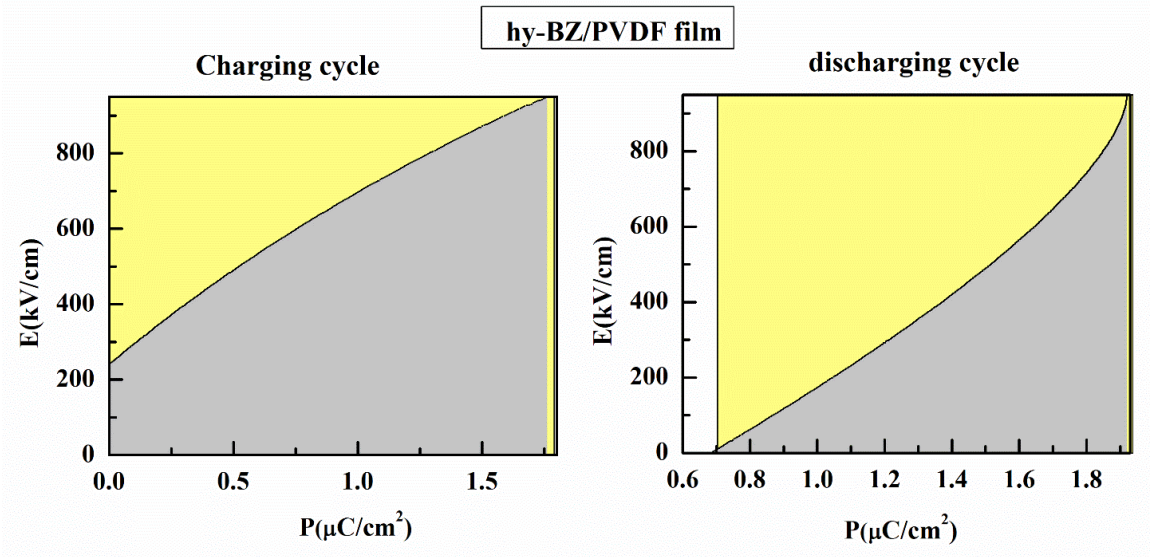

Fig.4.15 Partial PE hysteresis loop response for calculation of energy density for hy-BZ/PVDF film

Table 4.2 Comparison of the dielectric permittivity and energy storage density of different reported PVDF based Composites with hy-BZ/PVDF composite film.

Sample Name	**Dielectric permittivity**	**Energy storage density**	**Reference**
PVDF/Ag@BT	20	0.83	[203]
PVDF/hy-$LaFeO_3$	22	0.2	[142]
PVDF/$LaFeO_3$	8.5	-	[204]
BZ/PVDF	**16**	**0.77**	**Present work**
hy-BZ/PVDF	**26**	**1.11**	**Present work**

4.3.9 Weibull Analysis

Energy storage density is directly proportional to square of breakdown strength for linear dielectrics. Thus electric breakdown strength plays very crucial role in calculating the energy storage density of nanocomposites. The breakdown strength can be determined using Weibull analysis which is based on the plot between equation (4.1) and (4.2)

$$X_i = \ln(E_i) \tag{4.1}$$

$$Y_i = \ln[-\ln(1-i/(n+1))] \tag{4.2}$$

where X_i and Y_i are parameters in Weibull distribution, n is the total number of measurements, i is the ith number of sample/ measurement and E_i is the breakdown field of each sample. Serial number of sample can be decided by arranging them in ascending order of breakdown strength values. In Weibull distribution, X_i and Y_i have linear relationship where slope of the fitting line represents shape parameter β and average breakdown strength can be determined through the intersection point of fitting lines with horizontal line corresponding to $Y_i = 0$ [168]. Fig. 4.16 shows the Weibull distribution of

breakdown field measurement for pure PVDF film, BZ/PVDF film and hy-BZ/PVDF composite film and shape parameter is greater than 8. When a dielectric material with high dielectric constant are dispersed in the polymer matrix, an inhomogeneous electric field is created though out the composite material due to the sufficient large gap in the value of dielectric constant of filler and polymer which creates high local electric field around the fillers in the polymer than average electric field[205]. The average dielectric breakdown strength for BZ/PVDF and hy-BZ/PVDF was found to be 1287 kV/cm and 1495 kV/cm respectively. From this result, we see that average dielectric breakdown strength has been improved on hydroxylation of BZ particles.

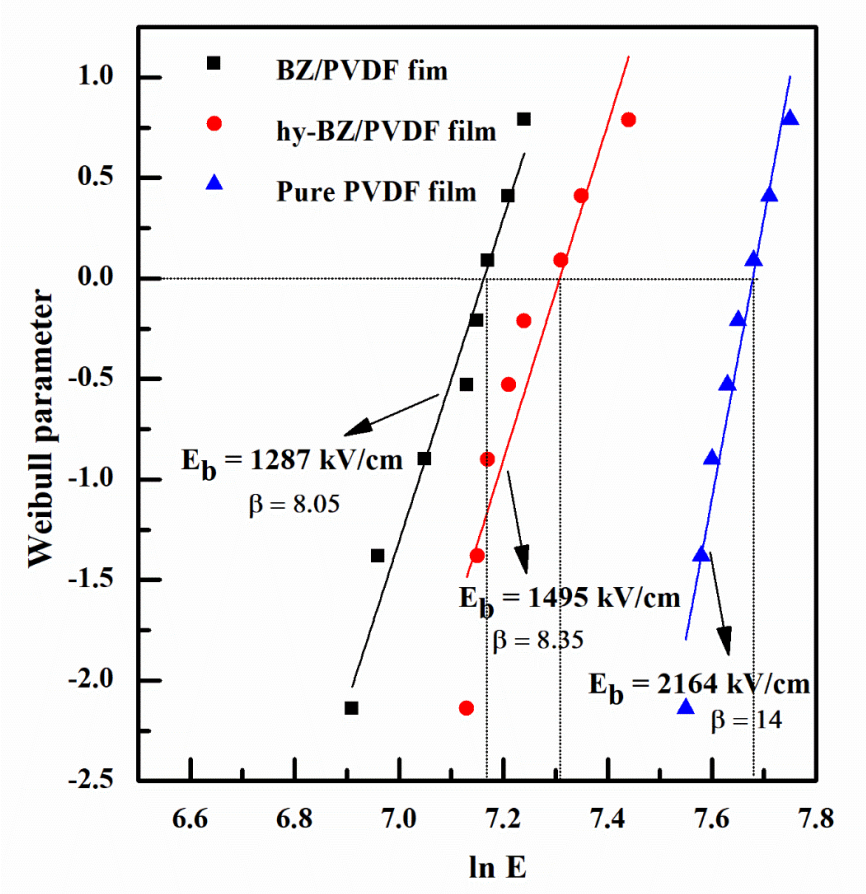

Fig. 4.16 Weibull analysis for PVDF film, BZ/PVDF and hy-BZ/PVDF composite film

4.4 Conclusion

We have successfully synthesized the $BaZrO_3$ nanoparticles followed by pure PVDF film, BZ/PVDF and hy-BZ/PVDF composite films using solution casting technique. FTIR spectra shows the successful hydroxylation of $BaZrO_3$ filler. TGA curve shows that there is no weight loss observed upto 450^0C in case of composites. The dielectric constant has been very much increased in case of hy-BZ/PVDF (ε_r ~26) in comparison to pure PVDF film (ε_r ~8) on the introduction of hydroxylated ceramic nanofiller in PVDF polymer matrix at room temperature. Polarization has been also increased upto almost double in case of hy-BZ/PVDF composite in comparison to pure PVDF film. We have achieved energy storage density 1.11 J/cm^3 for hy-BZ/PVDF composite much higher than the pure PVDF which is equal to 0.47 J/cm^3. Thus we can say that hy-BZ/PVDF is a potential material for dielectric capacitor application.